a minimum of ~ 1 μs on the supermolecule coherent lifetime T_c in using ^1H or ^2H reaction centers. Again, ESE is the advantageous method in comparison with EPR, ENDOR, or optical spectroscopy. According to ESE, the supermolecule dimer is coherent for at least 1 μs and again the coherent picture requires a picosecond dimeric species.

Summary and Conclusions

All measurements can be interpreted by considering the special pair as a symmetrical dimer on the picosecond time scale. The coherent delocalization interpretation of the magnetic resonance data demands a picosecond dimer in all cases. (We note in passing that the picosecond transient optical spectrum can still appear to be that of a nonstationary state monomer). The incoherent delocalization model can be interpreted in all cases in terms of a picosecond special pair, although only a nanosecond species is required by EPR or ENDOR. However, ESE results show the special pair cation must be a picosecond species for both incoherent or coherent models. This last statement is possible only because the ESE experiment on reversible processes provides spectroscopic data relevant to the subpicosecond time scale. Thus, from ESE measurements, we conclude that the chlorophyll special pair cation is a picosecond dimer.

Acknowledgment. We are grateful to Professor S. I. Weissman and Professor G. L. Closs for helpful discussions. J.R.N. appreciates many fruitful collaborations and discussions with Dr. J. J. Katz. This work was supported by the Office of Basic Energy Sciences, Division of Chemical Sciences, U.S. Department of Energy, under Contract W-31-109-Eng-38.

Resonance Raman Spectra and Vibrational Assignments of "Red" and "Black" Forms of Potassium Bis(dithiooxalato)nickel(II)

Roman S. Czernuszewicz,[†] Kazuo Nakamoto,*[†] and Dennis P. Strommen[‡]

Contribution from the Todd Wehr Chemistry Building, Marquette University, Milwaukee, Wisconsin 53233, and Department of Chemistry, Carthage College, Kenosha, Wisconsin 53141. *Received July 31, 1981*

Abstract: The infrared and Raman spectra of the red form of potassium bis(dithiooxalato)nickel(II) have been measured and complete vibrational assignments made on the basis of the ^{58}Ni-^{62}Ni isotope data and normal coordinate calculations. Resonance Raman spectra of the red form have provided two overtone series of the totally symmetric modes; $n_1\nu_1$ and $n_1\nu_1 + \nu_2$ where ν_1 is the C-C coupled with the C-S stretch and ν_2 is the C=O coupled with the C-C stretch. The calculated harmonic wavenumber and anharmonicity constant from the former series are 1088.5 ± 0.8 cm^{-1} and -1.74 ± 0.05 cm^{-1}, respectively. The differences in infrared and Raman spectra between the red and black forms have been interpreted in terms of molecular orbital and valence bond theories. Excitation profile studies of two totally symmetric vibrations (ν_1 and ν_4(Ni-S stretch)) of both forms reveal the presence of three electronic transitions in the visible region. The origin of these transitions has been discussed on the basis of previous molecular orbital calculations.

Potassium bis(dithiooxalato)nickel(II), $K_2[Ni(dto)_2]$, was first prepared and investigated by Robinson and Jones in 1912.[1] The salt which they obtained as dark red crystals from aqueous solution was first characterized via X-ray analysis by Cox et al.[2] Later Coucouvanis and his colleagues[3] refined the data and established that the red crystals were monoclinic (space group C_2/c) with $a = 22.52$ Å, $b = 7.86$ Å, $c = 11.09$ Å, and $\beta = 143.92°$. The dithiooxalate ion (dto^{2-}) is a versatile ligand that forms O,O-; S,S-; and O,S-bonded complexes where the coordination sites employed depend upon the "hardness" or "softness" of the metal.[4,5] In addition, it has the desirable property of being able to delocalize charge density throughout its relatively extensive π-orbital system. This latter property was one of the reasons that dto^{2-} ion was an early choice of Latham et al. in their quest for square-planar complexes of transition metals.[6] Following the discovery of the highly one-dimensional conducting system consisting of partially oxidized bis(oxalato)platinum[7,8] and unsuccessful attempts to synthesize similar Pt systems with the dto^{2-} ion as the ligand, Gleizes et al.[9] substituted Ni for Pt and attempted to obtain a partially oxidized form of $[Ni(dto)_2]^{2-}$. Although they claimed to be able to detect a partially oxidized species in acetone solution, they were unable to isolate it. However, when using $K_2Cr_2O_7$ as an oxidant they obtained a black, crystalline material which was subsequently shown to correspond to the formula $K_2[Ni(dto)_2]$. X-ray analysis revealed that the crystals have monoclinic symmetry (space group $P2_1/n$) with $a = 11.04$ Å, $b = 4.19$ Å, $c = 12.72$ Å, and $\beta = 111.78°$. In both cases, the $[Ni(dto)_2]^{2-}$ moiety is planar, but in the black crystals it is tilted with respect to the stacking axis.

In this paper we report the results of a detailed IR and Raman investigation of these two fascinating compounds. Included in the above are complete band assignments obtained from a normal coordinate analysis of the red form of $K_2[Ni(dto)_2]$, calculated values for the anharmonicity constant of the ν_1 mode (C-C coupled with C-S stretch), obtained from overtone progressions in resonance Raman spectra as well as verification of earlier MO calculations[6] through the use of Raman excitation profiles.

[†] Marquette University.
[‡] Carthage College.

(1) Robinson, C. S.; Jones, H. O. *J. Chem. Soc.* **1912**, *101*, 62.
(2) Cox, E. G.; Wardlaw, W.; Webster, K. C. *J. Chem. Soc.* **1935**, 1475.
(3) Coucouvanis, D.; Baenziger, N. C.; Johnson, S. M. *J. Am. Chem. Soc.* **1973**, *95*, 3875.
(4) Coucouvanis, D. *J. Am. Chem. Soc.* **1970**, *92*, 707.
(5) Coucouvanis, D.; Piltingsrud, D. *J. Am. Chem. Soc.* **1973**, *95*, 5556.
(6) Latham, A. R.; Hascall, V. C.; Gray, H. B. *Inorg. Chem.* **1965**, *4*, 788.
(7) Lecrone, F. N.; Minot, M. J.; Perlstein, J. H. *Inorg. Nucl. Chem. Lett.* **1972**, *8*, 173.
(8) Thomas, T. W.; Hsu, C.; Labes, M. M.; Gomm, P. S.; Underhill, A. E.; Watkins, D. M. *J. Chem. Soc., Dalton Trans.* **1972**, 2050.
(9) Gleizes, A.; Clery, F.; Bruniquel, M. F.; Cassoux, P. *Inorg. Chim. Acta* **1979**, *37*, 19.

0002-7863/82/1504-1515$01.25/0

Table I. Observed and Calculated Frequencies (cm^{-1}) and Band Assignments for the $[Ni(S_2C_2O_2)_2]^{2-}$ Ion[a]

	obsd	calcd	predominant mode[b]	potential energy distribution, %
			A_g Species	
ν_1	1085	1085.8	ν(C–C) + ν(C–S)	$S_4(48) + S_2(38)$
ν_2	1602	1601.9	ν(C=O) + ν(C–C)	$S_1(82) + S_4(11)$
ν_3	607	608.1	ν(C=S) + ν(C–C) + ν(C=O) + ring def	$S_2(50) + S_4(21) + S_1(14) + S_7(11)$
ν_4	317	316.4	ν(Ni–S) + δ(O=C–S) + ring def	$S_3(54) + S_5(21) + S_6(23)$
ν_5	238	237.3	ring def + δ(O=C–S) + ν(Ni–S)	$S_7(33) + S_5(30) + S_3(29)$
ν_6	131	131.1	ring def	$S_7(52) + S_6(43)$
			B_{1g} Species	
ν_7	1585	1584.9	ν(C=O) + ring def	$S_8(77) + S_{13}(11)$
ν_8	933	932.2	ν(C–S) + δ(O=C–S)	$S_9(64) + S_{11}(25)$
ν_9	417	416.9	ring def	$S_{13}(80)$
ν_{10}	398	399.7	δ(O=C–S) + ν(C–S)	$S_{11}(70) + S_9(20)$
ν_{11}	207	208.7	ν(Ni–S) + ring def	$S_{10}(79) + S_{12}(13)$
			B_{2u} Species	
ν_{12}	1602	1602.3	ν(C=O) + ν(C–C)	$S_{14}(82) + S_{17}(11)$
ν_{13}	1084	1085.1	ν(C–C) + ν(C–S)	$S_{17}(48) + S_{15}(38)$
ν_{14}	615	614.3	ν(C–S) + ν(C–C) + ν(C=O) + ring def	$S_{15}(48) + S_{17}(19) + S_{14}(14) + S_{20}(15)$
ν_{15}	362 (7.0)	361.8 (7.3)	ν(Ni–S) + δ(SNiS)	$S_{16}(67) + S_{20}(29)$
ν_{16}	265 (1.0)	264.6 (1.1)	δ(O=C–S) + δ(SNiS)	$S_{18}(65) + S_{20}(20)$
ν_{17}	176 (0.0)	174.4 (0.4)	ring def + δ(SNiS)	$S_{19}(58) + S_{20}(29)$
			B_{3u} Species	
ν_{18}	1585	1584.9	ν(C=O) + ring def	$S_{21}(77) + S_{26}(11)$
ν_{19}	933	932.6	ν(C–S) + δ(O=C–S)	$S_{22}(64) + S_{24}(25)$
ν_{20}	435 (2.0)	435.9 (2.5)	ring def + ν(Ni–S)	$S_{26}(58) + S_{23}(32)$
ν_{21}	408 (1.0)	407.9 (0.7)	δ(O=C–S) + ring def + ν(Ni–S)	$S_{24}(45) + S_{26}(22) + S_{23}(15)$
ν_{22}	352.6 (5.1)	352.4 (4.8)	ν(Ni–S) + δ(O=C–S) + ring def	$S_{23}(45) + S_{24}(18) + S_{25}(20)$
ν_{23}		49.1	δ(SNiS) + ν(Ni–S)	$S_{27}(66) + S_{23}(27)$

[a] Numbers in parentheses indicate isotopic shifts, $\nu(^{58}Ni) - \nu(^{62}Ni)$. [b] ν, stretching; δ, in-plane bending.

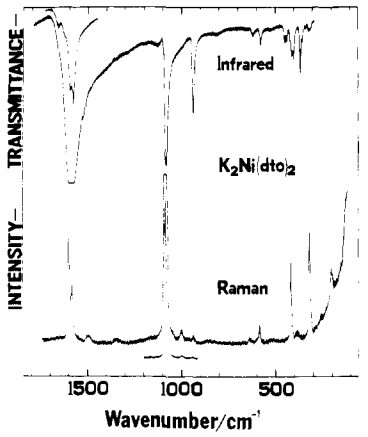

Figure 1. IR and Raman (457.9-nm excitation) spectra of the red form of $K_2[Ni(dto)_2]$.

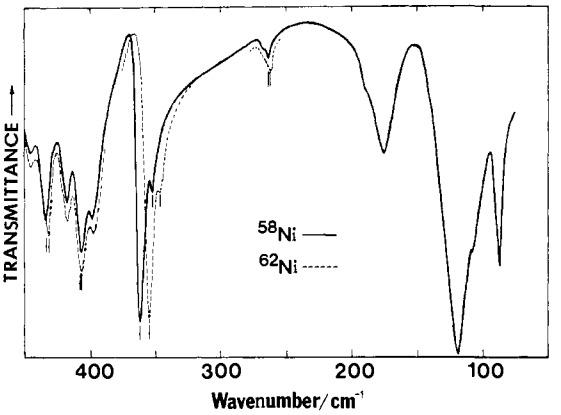

Figure 2. Far-IR spectra of red $K_2[^{58}Ni(dto)_2]$ and its ^{62}Ni analogue.

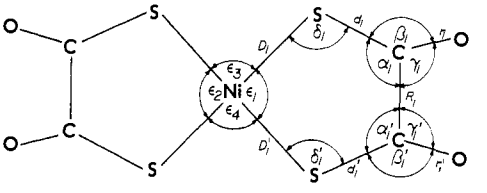

Figure 3. Structure and internal coordinates of the $[Ni(dto)_2]^{2-}$ ion.

Experimental Section

Preparation of Compounds. The red form of $K_2[Ni(dto)_2]$ was prepared according to the literature.[1,2] The black form of $K_2[Ni(dto)_2]$ was obtained from the red form following the method described by Gleizes et al.[9] Elemental ^{58}Ni and ^{62}Ni were first converted to chlorides and finally to the corresponding dto complexes.

Physical Measurements. Infrared spectra of the solids were recorded with the materials suspended in KBr pellets by using a Beckman IR 4260 spectrophotometer. The far-infrared spectra of $K_2[^{58}Ni(dto)_2]$ and $K_2[^{62}Ni(dto)_2]$ were measured as Nujol mulls on a Nicolet FTIR-7199 spectrometer at Northwestern University, Evanston, IL. Electronic spectra were recorded on a Cary Model 14 spectrophotometer. Exciting radiation for Raman spectra was provided by a Spectra-physics Model 164 Ar-ion laser powered by a Model 265 exciter (457.9–514.5 nm) and a Spectra-Physics Model 365 CW dye laser pumped by the Ar-ion laser. Dyes employed in the latter were Rhodamine 6G (570.0–620.0 nm) and sodium fluorescein (535.0–570.0 nm). The sodium fluorescein solution was prepared by dissolving 1.00 g in 750 mL of ethylene glycol with 2.5 mL of cyclooctatetraene. The scattered radiation was dispersed by a Spex 1401 double monochromator and detected by a cooled RCA 31034A photomultiplier using a Spex DPC2 photon counting system. All samples were rotated to avoid thermal decomposition. The $K_2[Ni(dto)_2]$ complexes were run as 5.00×10^{-4} M solutions in acetone or water (to compare intensities, the 791-cm^{-1} band of acetone was used as an internal standard) as well as in the solid state on the surface of a rotating KBr disk. Depolarization ratios were determined at each wavelength by analyzing the scattered light in front of the monochromator slit with a polarizer and a polarization scrambler. When constructing excitation profiles the signals were corrected for the ν^4 dependence of scattered radiation, self-absorption, and spectrophotometer response at each wavelength. The corrected intensities were then normalized relative to the intensities obtained at 611.2- (red form) and 457.9-nm (black form) excitation and plotted for comparison with their respective electronic spectra.

Results and Discussion

Red Form of $K_2[Ni(dto)_2]$: Vibrational Spectra and Normal Coordinate Analysis. Figure 1 shows the IR and Raman spectra

Table II. Bond Distances and Angles of the $[Ni(S_2C_2O_2)_2]^{2-}$ Ion[a]

bond distance, Å	angle, deg
$D = 2.1795$	$\alpha = 117.5$
$d = 1.750$	$\beta = 124.0$
$R = 1.5450$	$\gamma = 118.5$
$r = 1.2065$	$\delta = 106$
	$\epsilon_1 = 92.9$
	$\epsilon_3 = 87.1$

[a] Taken from ref 3.

of $K_2[Ni(dto)_2]$, and Figure 2 shows the far-IR spectra of $K_2[^{58}Ni(dto)_2]$ and its ^{62}Ni analogue. The frequencies of all the bands observed in the IR and Raman spectra are listed in Table I.

In order to make accurate assignments of the observed bands, we have carried out normal coordinate analysis on the whole $[Ni(dto)_2]^{2-}$ ion shown in Figure 3. The present calculation is much more complete than the previous work[10] in which calculations were made on a simple 1:1 metal/ligand model without Raman data. Table II lists the molecular parameters[3] used for our calculations.

Thirty three normal vibrations of the $[Ni(dto)_2]^{2-}$ ion are spanned by $6A_g + 5B_{1g} + 2B_{2g} + 2B_{3g} + 3A_u + 3B_{1u} + 6B_{2u} + 6B_{3u}$ under D_{2h} symmetry. They can be readily separated into 23 in-plane vibrations ($6A_g + 5B_{1g} + 6R_{2u} + 6B_{3u}$) and 10 out-of-plane vibrations ($3A_u + 3B_{1u} + 2B_{2g} + 2B_{3g}$). In the present paper, we have calculated frequencies for the 23 inplane vibrations using the programs developed by Schachtschneider.[11] The symmetry coordinates for the A_g, B_{1g}, B_{2u}, and B_{3u} vibrations are listed in Table III. Seven redundancies involving angle bending coordinates of the chelate rings were removed by a similarity transformation. The four remaining redundancies are included in the 27 symmetry coordinates listed in Table III. The potential energy was expressed by a modified Urey–Bradley force field which included bond stretching (K), angle bending (H), repulsive (F), and selected general valence interaction (f) force constants. The matrix secular equation of the form $|GF - E\lambda| = 0$ were solved for each species with a Xerox Sigma 9 computer. The single redundancy that remained in each species produced zero frequency in the final result.

The calculated force constants are listed in Table IV. In Table I, the frequencies calculated from this set of force constants are compared with the values observed for the $[Ni(dto)_2]^{2-}$ ion. The calculated frequencies are in excellent agreement with the observed values with an average error of less than 1%. Assignments of vibrational modes have been made on the basis of the evaluation of the potential-energy distribution in each normal vibration. The fourth and fifth columns of Table I give the predominant mode and the potential-energy distribution, respectively. It is seen that there is considerable mixing of the symmetry coordinates in most of these normal vibrations.

Infrared-Active Modes. As is seen in the upper trace of Figure 1, $K_2[Ni(dto)_2]$ exhibits strong bands at 1602 (ν_{12}), 1585 (ν_{18}), 1084 (ν_{13}), and 933 cm^{-1} (ν_{19}) in its IR spectrum. Table I indicates that former two are mainly ν(C=O) of the B_{2u} and B_{3u} species, respectively, whereas the latter two are strongly coupled vibrations; the band at 1084 cm^{-1} (ν_{13}) is attributed to coupling of the ν(C–C) and ν(C–S) stretching vibrations (B_{2u} species), while the band at 933 cm^{-1} (ν_{19}) results from coupling of the ν(C—S) with δ(O=C—S) vibrations (B_{3u} species). The weak band appearing at 615 cm^{-1} (ν_{14}) is assigned to a B_{2u} ν(C—S) strongly coupled with ν(C—C), ν(C=O) and a ring deformation mode.

In general our assignments above 500 cm^{-1} are similar to those reported previously for the $[Pt(dto)_2]^{2-}$ ion.[10] Marked differences in the assigments occur below 500 cm^{-1} where the B_{2u} and B_{3u} ν(Ni–S) are expected to appear. Previously, the bands at 432 and ca. 360 cm^{-1} were assigned to ν(Ni–S) and δ(C–O), respectively.[10]

(10) Fujita, J.; Nakamoto, K. *Bull. Chem. Soc. Jpn.* **1964**, *37*, 528.
(11) Schachtschneider, J. H. "Vibrational Analysis of Polyatomic Molecules"; Shell Development Co.: Emeryville, CA, 1964, 1965; Vol. V and VI, Technical Reports No. 231-64 and 57-61.

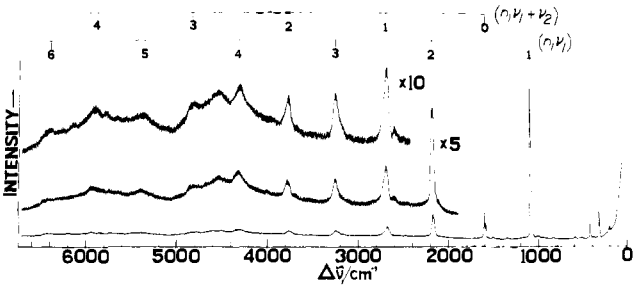

Figure 4. RR spectra of red $K_2[Ni(dto)_2]$ in the solid state (488.0-nm excitation).

However, Coucouvanis et al.[3] reported that only the band near 360 cm^{-1} was shifted by ^{58}Ni–^{62}Ni isotopic substitution. Thus they reversed the previous assignments. Our far-IR spectra of isotopically substituted $K_2[Ni(dto)_2]$ (Figure 2) show significant isotopic shifts at 362.0 and 352.6 cm^{-1} as well as 435.0 cm^{-1}. The mode structures of the two former bands as seen in Table I are dominated by Ni–S stretching coordinates mixed with lesser amounts of ring bending while the latter is predominantly made up of ring bending but with a significant contribution (32%) from S_{23}, a Ni–S stretching coordinate. The bands at 408 (ν_{21}) and 265 cm^{-1} (ν_{16}) are the δ(O=C—S) coupled with a ring deformation and ν(Ni—S) and with δ(S—Ni—S), respectively. These two bands show small shifts (1 cm^{-1}) by the ^{58}Ni–^{62}Ni substitution. It is clear from the above discussion that care must be taken when assigning low frequency modes in the absence of good normal coordinate analyses as well as metal isotope data.

Raman-Active Modes. The lower trace of Figure 1 shows the Raman spectrum of $K_2[Ni(dto)_2]$ obtained by using the 457.9-nm line. This wavelength was chosen to minimize the resonance Raman effect which will be discussed later.

There is one very intense band at 1085 cm^{-1} (ν_1), four medium bands at 1602 (ν_2), 1585 (ν_7), 417 (ν_9), and 317 cm^{-1} (ν_4), and a few weak bands at 933 (ν_8), 607 (ν_3), 398 (ν_{10}), 237 (ν_5), 207 (ν_{11}), and 131 cm^{-1} (ν_6). Table I indicates that the strongest band [1085 cm^{-1} (ν_1)] is attributed to coupled ν(C–C) + ν(C–S). The predicted position of this band coincides nicely with that of the $\nu_{13}(B_{2u})$ ν(C–C) + ν(C–S) observed in the IR spectrum. The bands at 1602 (ν_2) and 1585 cm^{-1} (ν_7) are nearly pure ν(C=O) modes belonging to the A_g and B_{1g} species, respectively. They correspond exactly to the $\nu_{12}(B_{2u})$ and $\nu_{18}(B_{3u})$ bands observed in the IR spectrum. The weak band at 933 cm^{-1} (ν_8) is due to the coupling of the ν(C—S) and δ(O=C—S) in the B_{1g} species.

According to Table I, the medium intensity band at 317 cm^{-1} (ν_4) and a weak band at 207 cm^{-1} (ν_{11}) are assigned to the ν(Ni–S) coupled with ring deformation modes. These frequencies do not coincide with the corresponding ν(Ni–S) in the IR spectrum (ν_{15} and ν_{22}). Thus, due to the strong coupling of interligand Ni–S motions, the mutual exclusion rule holds for the ν(Ni–S) frequencies as expected for a molecule of D_{2h} symmetry.

Resonance Raman Spectra and Anharmonicity Constant Calculations. Figure 4 shows the RR spectra of the red form of $K_2[Ni(dto)_2]$ in the solid state. Two series of overtones are clearly seen as indicated on the abscissa scale: the $n_1\nu_1$ progression (up to $n_1 = 6$) and $n_1\nu_1 + \nu_2$ progression (up to $n_1 = 4$). The wavenumbers of each member of these progressions are given in Table V.

Previously, Clark and co-workers measured the RR spectra of the tetrahedral MX_4-type ions[12] and M_2X_8-type metal clusters[13] and observed a series of long overtone progressions of the totally symmetric vibrations in each case. The present result is unique in that its fundamental frequency is much higher than those studied by Clark et al. (below 500 cm^{-1}).[12,13]

The observation of a number of overtones of the ν_1 fundamental in the RR spectra of $K_2[Ni(dto)_2]$ makes it possible to determine the harmonic wavenumber (ω_1) and anharmonicity constant (X_{11}).

(12) Clark, R. J. H.; Mitchell, P. D. *J. Am. Chem. Soc.* **1973**, *95*, 8300.
(13) Clark, R. J. H.; Franks, M. *J. Chem. Soc.* **1974**, 316.

Table III. Symmetry Coordinates for the $[Ni(S_2C_2O_2)_2]^{2-}$ Ion[a]

A_g Species	
$S_1 = (1/2)(\Delta r_1 + \Delta r_1' + \Delta r_2 + \Delta r_2')$	ν(C=O)
$S_2 = (1/2)(\Delta d_1 + \Delta d_1' + \Delta d_2 + \Delta d_2')$	ν(C–S)
$S_3 = (1/2)(\Delta D_1 + \Delta D_1' + \Delta D_2 + \Delta D_2')$	ν(Ni–S)
$S_4 = (1/\sqrt{2})(\Delta R_1 + \Delta R_2)$	ν(C–C)
$S_5 = (1/2\sqrt{2})[(\Delta\beta_1 - \Delta\gamma_1 + \Delta\beta_1' - \Delta\gamma_1') + (\Delta\beta_2 - \Delta\gamma_2 + \Delta\beta_2' - \Delta\gamma_2')]$	δ(O=C–S)
$S_6 = (1/2\sqrt{2})[(\Delta\alpha_1 + \Delta\alpha_1' - \Delta\delta_1 - \Delta\delta_1') + (\Delta\alpha_2 + \Delta\alpha_2' - \Delta\delta_2 - \Delta\delta_2')]$	ring def
$S_7 = (1/10)[(-\Delta\alpha_1 - \Delta\alpha_1' - \Delta\delta_1 - \Delta\delta_1' + 4\Delta\epsilon_1 - 5\Delta\epsilon_3) + (-\Delta\alpha_2 - \Delta\alpha_2' - \Delta\delta_2 - \Delta\delta_2' + 4\Delta\epsilon_2 - 5\Delta\epsilon_4)]$	ring def
B_{1g} Species	
$S_8 = (1/2)(\Delta r_1 - \Delta r_1' - \Delta r_2 + \Delta r_2')$	ν(C=O)
$S_9 = (1/2)(\Delta d_1 - \Delta d_1' - \Delta d_2 + \Delta d_2')$	ν(C–S)
$S_{10} = (1/2)(\Delta D_1 - \Delta D_1' - \Delta D_2 + \Delta D_2')$	ν(Ni–S)
$S_{11} = (1/2\sqrt{2})[(\Delta\beta_1 - \Delta\gamma_1 - \Delta\beta_1' + \Delta\gamma_1') - (\Delta\beta_2 - \Delta\gamma_2 - \Delta\beta_2' + \Delta\gamma_2')]$	δ(O=C–S)
$S_{12} = (1/2\sqrt{2})[(\Delta\alpha_1 - \Delta\alpha_1' + \Delta\delta_1 - \Delta\delta_1') - (\Delta\alpha_2 - \Delta\alpha_2' + \Delta\delta_2 - \Delta\delta_2')]$	ring def
$S_{13} = (1/2\sqrt{2})[(\Delta\alpha_1 - \Delta\alpha_1' - \Delta\delta_1 + \Delta\delta_1') - (\Delta\alpha_2 - \Delta\alpha_2' - \Delta\delta_2 + \Delta\delta_2')]$	ring def
B_{2u} Species	
$S_{14} = (1/2)(\Delta r_1 + \Delta r_1' - \Delta r_2 - \Delta r_2')$	ν(C=O)
$S_{15} = (1/2)(\Delta d_1 + \Delta d_1' - \Delta d_2 - \Delta d_2')$	ν(C–S)
$S_{16} = (1/2)(\Delta D_1 + \Delta D_1' - \Delta D_2 - \Delta D_2')$	ν(Ni–S)
$S_{17} = (1/\sqrt{2})(\Delta R_1 - \Delta R_2)$	ν(C–C)
$S_{18} = (1/2\sqrt{2})[\Delta\beta_1 - \Delta\gamma_1 + \Delta\beta_1' - \Delta\gamma_1') - (\Delta\beta_2 - \Delta\gamma_2 + \Delta\beta_2' - \Delta\gamma_2')]$	δ(O=C–S)
$S_{19} = (1/2\sqrt{2})[\Delta\alpha_1 + \Delta\alpha_1' - \Delta\delta_1 - \Delta\delta_1') - (\Delta\alpha_2 + \Delta\alpha_2' - \Delta\delta_2 - \Delta\delta_2')]$	ring def
$S_{20} = (1/5\sqrt{2})[(-\Delta\alpha_1 - \Delta\alpha_1' - \Delta\delta_1 - \Delta\delta_1' + 4\Delta\epsilon_1) - (-\Delta\alpha_2 - \Delta\alpha_2' - \Delta\delta_2 - \Delta\delta_2' + 4\Delta\epsilon_2)]$	δ(SNiS)
B_{3u} Species	
$S_{21} = (1/2)(\Delta r_1 - \Delta r_1' + \Delta r_2 - \Delta r_2')$	ν(C=O)
$S_{22} = (1/2)(\Delta d_1 - \Delta d_1' + \Delta d_2 - \Delta d_2')$	ν(C–S)
$S_{23} = (1/2)(\Delta D_1 - \Delta D_1' + \Delta D_2 - \Delta D_2')$	ν(Ni–S)
$S_{24} = (1/2\sqrt{2})[(\Delta\beta_1 - \Delta\gamma_1 - \Delta\beta_1' + \Delta\gamma_1') + (\Delta\beta_2 - \Delta\gamma_2 - \Delta\beta_2' + \Delta\gamma_2')]$	δ(O=C–S)
$S_{25} = (1/2\sqrt{2})[(\Delta\alpha_1 - \Delta\alpha_1' + \Delta\delta_1 - \Delta\delta_1') + (\Delta\alpha_2 - \Delta\alpha_2' + \Delta\delta_2 - \Delta\delta_2')]$	ring def
$S_{26} = (1/2\sqrt{2})[(\Delta\alpha_1 - \Delta\alpha_1' - \Delta\delta_1 + \Delta\delta_1') + (\Delta\alpha_2 - \Delta\alpha_2' - \Delta\delta_2 + \Delta\delta_2')]$	ring def
$S_{27} = (1/\sqrt{2})(\Delta\epsilon_3 - \Delta\epsilon_4)$	δ(SNiS)

[a] ν, stretching mode; δ, in-plane bending mode.

Table IV. Force Constants (mdy/Å) for the $[Ni(S_2C_2O_2)_2]^{2-}$ Ion

K(C=O)	8.70	$H(\Delta\epsilon)$	0.10	$f(D_1,D_2')$	0.12
K(C–S)	3.65	F(S···S)	0.06	$f(r_1,R_1)$	−0.14
K(Ni–S)	1.18	F(Ni···C)	0.04	$f(D_1,\epsilon_1)$	−0.10
K(C–C)	2.76	F(S···C)	0.63	$f(D_1,\epsilon_3)$	−0.20
H($\Delta\alpha$)	0.27	F(O···S)	0.25	$f(D_1,\delta_1)$	0.20
H($\Delta\beta$)	0.45	F(C···O)	0.15	$f(\beta_1,\gamma_1)$	0.04
H($\Delta\gamma$)	0.45	$f(D_1,D_1')$	−0.15	$f(\gamma_1,\gamma_1')$	−0.08
H($\Delta\delta$)	0.10	$f(D_1,D_2)$	0.15		

Table V. Wavenumbers of the $n_1\nu_1$ and $n_1\nu_1 + \nu_2$ Progressions in the Resonance Raman Spectrum of $K_2[Ni(dto)_2]$ (488.0-nm Excitation)

$n_1\nu_1$ progression		$n_1\nu_1 + \nu_2$ progression	
band	wave no., cm^{-1}	band	wave no., cm^{-1}
ν_1	1085	$\nu_1 + \nu_2$	2685
$2\nu_1$	2167	$2\nu_1 + \nu_2$	3766
$3\nu_1$	3245	$3\nu_1 + \nu_2$	4842
$4\nu_1$	4318	$4\nu_1 + \nu_2$	5924
$5\nu_1$	5390		
$6\nu_1$	6460		

In general, the observed wavenumber $\nu(n_1)$, of any overtone of the ν_1 fundamental, is given by the expression[14]

$$\nu(n_1) = G_1(n_1) - G(0) = n_1\omega_1 + X_{11}(n_1^2 + n_1d_1) + \dots \quad (1)$$

where $G(n_1)$ is the term value of the n_1th vibrational level, and n_1 and d_1 are the vibrational quantum number and degeneracy, respectively, of this fundamental. With the simplification that $d_1 = 1$ (since ν_1 is totally symmetric and consequently nondegenerate), a plot of $\nu(n_1)/n_1$ vs. n_1 will then give a straight line with a slope equal to X_{11} and an intercept equal to $\omega_1 + X_{11}$.

(14) Herzberg, G. "Infrared and Raman Spectra of Polyatomic Molecules"; Van Nostrand: New York, 1945; p 205.

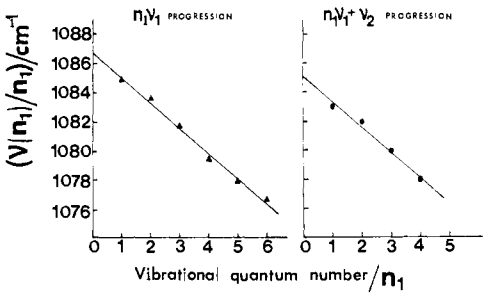

Figure 5. Plots of $\nu(n_1)/n_1$ vs. n_1 for $n_1\nu_1$ and $n_1\nu_1 + \nu_2$ progressions for red $K_2[Ni(dto)_2]$.

Table VI. Harmonic Wavenumbers (ω_1) and Anharmonicity Constants (X_{11}) for $K_2[Ni(dto)_2]$ (cm^{-1})

	$n_1\nu_1$ progression	$n_1\nu_1 + \nu_2$ progression
ω_1	1088.5 ± 0.8	1086.7 ± 0.9
X_{11}	−1.74 ± 0.05	−1.70 ± 0.06

It is also possible to observe a progression of the type $(n_1\nu_1 + \nu_2)$, which is given by the expression

$$\nu(n_1\nu_1 + \nu_2) = G_1(n_1,n_2) - G(0, n_2 - 1) = n_1\omega_1 + \omega_2 + X_{11}(n_1^2 + n_1d_1) + X_{22}(2n_2 - 1 + d_2) + X_{12}(n_1n_2 + n_1(d_2/2) + (d_1/2)) + \dots \quad (2)$$

Since the observed wavenumber of the ν_2 fundamental is given by the expression

$$\nu_2 = G(n_1,n_2) - G(n_1,n_2 - 1) = \omega_2 + X_{22}(2n_2 - 1 + d_2) + X_{12}(n_1 + (d_1/2)) + \dots \quad (3)$$

we obtain the following equation:

$$\nu(n_1\nu_1 + \nu_2) - \nu_2 = n_1\omega_1 + X_{11}(n_1^2 + n_1d_1) + n_1X_{12}(n_2 - 1 + (d_2/2)) + \dots \quad (4)$$

A plot of $[\nu(n_1\nu_1 + \nu_2) - \nu_2]/n_1$ vs. n_1 gives the same slope, X_{11},

Table VII. Bond Distances and Infrared and Raman Frequencies of Red and Black $K_2[Ni(dto)_2]$ and $(BzPh_3P)_2[Ni(dto)_2(SnCl_4)_2]$

compound	bond distance,[a] Å	IR, cm^{-1}	Raman, cm^{-1}	assignment
red $K_2[Ni(dto)_2]$[b]	C=O, 1.206	1602	1602	ν(C=O)
		1585	1585	
	C–S, 1.750	1084	1085	ν(C–C) + ν(C–S)
	C–C, 1.545			
	Ni–S, 2.180	362	317	ν(Ni–S)
black $K_2[Ni(dto)_2]$[b]	C=O, 1.234	1505	1504	ν(C=O)
		1490	1488	
	C–S, 1.707	1144	1149	ν(C–S) + ν(C–S)
	C–C, 1.540			
	Ni–S, 2.183	374	329	ν(Ni–S)
$(BzPh_3P)_2[Ni(dto)_2(SnCl_4)_2]$[c]	C=O, 1.264	1469	1490	ν(C=O)
	C–S, 1.670	1150	1155	ν(C–C) + ν(C–S)
	C–C, 1.513			
	Ni–S, 2.183	378	335	ν(Ni–S)

[a] Average of two bond distances. [b] Bond distances from ref 9. [c] Bond distances from ref 3.

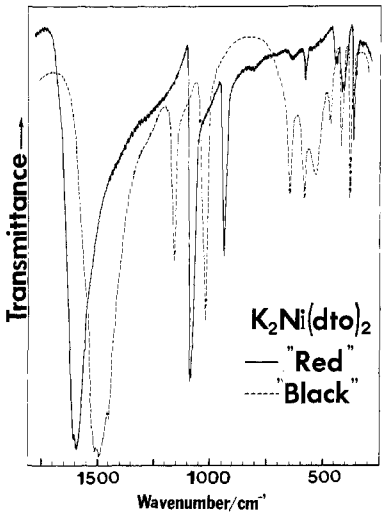

Figure 6. Comparison of IR spectra of black and red $K_2[Ni(dto)_2]$.

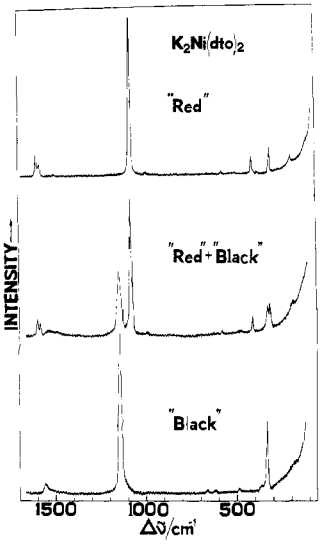

Figure 7. RR spectra of red and black $K_2[Ni(dto)_2]$ and their mixture (488.0-nm excitation).

as that of a plot of $\nu(n_1)/n_1$ vs. n_1, but it differs in its intercept precisely by the quantity X_{12}.

Extensive work in this area[15] has shown that the compounds which display long $n_1\nu_1$ progressions are invariably ones whose bonds have a high degree of covalent character or with a bond order greater than one. Our detailed RR studies of $K_2[Ni(dto)_2]$ offer an opportunity to carry out a similar analysis. The experimental results for $K_2[Ni(dto)_2]$ are shown in Figure 5, and the ω_1 and X_{11} values obtained by a least-squares analysis are shown in Table VI. The X_{11} value, -1.74 ± 0.05 cm^{-1}, is significantly larger than those reported for other modes[15] which exhibit progressions in RR spectra. However, the ratio X_{11}/ω_1 (1.6×10^{-3}) is very small. Thus the ν_1 mode closely approximates a harmonic oscillator. The values for ω_1 and X_{11} were also deduced from the wavenumbers of the $n_1\nu_1 + \nu_2$ progression by plotting $[\nu(n_1\nu_1 + \nu_2) - \nu_2]/n_1$ vs. n_1 (Figure 5). The value of 1602 cm^{-1} for $\nu_2(A_g)$ was used for this plot. As is seen in Table VI, the X_{11} value so obtained (-1.70 ± 0.06 cm^{-1}) agrees within experimental error with that deduced from the $n_1\nu_1$ progression. However, the ω_1 value derived from the $n_1\nu_1$ progression is 1.7 cm^{-1} larger than that derived from the $n_1\nu_1 + \nu_2$ progression. This difference gives the cross-term X_{12} in eq 4. Thus X_{12} is similar in magnitude to that of X_{11}.

Comparison of Red and Black Forms of $K_2[Ni(dto)_2]$. Vibrational Spectra. As mentioned in the introduction, there are two polymorphic forms of $K_2[Ni(dto)_2]$. Table VII contains selected bond distances for the red and black $K_2[Ni(dto)_2]$ complexes together with associated stretching frequencies from their IR and RR spectra. Figure 6 shows the IR spectra of these complexes while Figure 7 shows their RR spectra as well as a spectrum of a mixture of the two.

The IR and RR spectra of these two forms differ primarily in the positions of three sets of bands. According to the previous section, the bands between 1585 and 1602 cm^{-1} (ν_2, ν_7, ν_{12}, and ν_{18}) in the red form are predominantly ν(C=O), while a second set at 1084 cm^{-1} (ν_{13}, IR) and 1085 cm^{-1} (ν_1, RR) are attributed to coupled ν(C–C) + ν(C–S). In the corresponding IR and Raman spectra of the black $K_2[Ni(dto)_2]$, the ν(C=O) vibrations occur between 1488 and 1500 cm^{-1} while the band due to the coupled ν(C–C) + ν(C–S) is found at 1144 (IR) cm^{-1}. These observed frequency shifts are completely consistent with the bond length changes reported in the X-ray data (see Table VII). As the C=O bond distance increases, the frequencies of those modes which involve C=O stretching decrease (e.g., ν_2, 1602–1505 cm^{-1}) while the opposite effect is observed in the C–S stretching region (ν_1, 1055–1145 cm^{-1}).

The third spectral region where significant changes are observed is at low frequency where the Ni–S stretching vibrations are expected to occur. The red complex has bands at 362 cm^{-1} (IR) and 317 cm^{-1} (RR) which contain significant contributions from ν(Ni–S) (Table I). The corresponding bands in the black complex are found at 374 and 329 cm^{-1}, respectively. On the basis of X-ray data, these shifts are quite unexpected since, as can be seen in Table VII, the Ni–S bond distances are nearly identical in both compounds. However, as Jones[16] pointed out some 20 years ago, force constants and thus vibrational frequencies are extremely

(15) Clark, R. J. H.; Stewart, B. *Struct. Bonding (Berlin)* **1979**, *36*, 1.

(16) Jones, L. H. *Spectrochim. Acta* **1959**, *6*, 409.

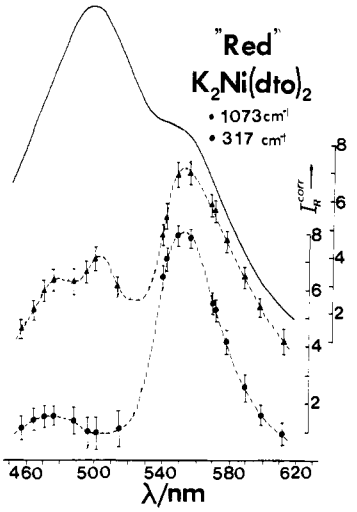

Figure 8. Excitation profiles and electronic spectrum of red $K_2[Ni(dto)_2]$.

sensitive measures of bond length.

When the stannic halide adducts of the red form of $K_2[Ni(dto)_2]$ are prepared and studied, even more dramatic shifts are observed (see, for example, Table VII and ref 3). Comparison of the IR and RR spectra of red $K_2[Ni(dto)_2]$ with that of $(BzPh_3P)_2[Ni(dto)_2(SnCl_4)_2]$ reveals that the C=O stretching band shifts down by 66 cm^{-1} while the ν(C=C) coupled with ν(C—S) band shifts upward by 70 cm^{-1} and the band identified as ν(Ni—S) jumps 17 cm^{-1}. Since the stannic halides are known to bind to the oxygen atoms of the dto moiety and to delocalize charge toward the stannic halide,[3] we can appeal to the results of molecular orbital studies to account for the observed spectral shifts.[6,17] The ground-state molecular orbital involves overlap of the Ni-4s and the S-σ orbitals as well as the metal d_{xz} (d_{yz}) with a π orbital located on the S atom. As electrons are delocalized toward the oxygen end of the dto, the S → Ni σ bonding will decrease but apparently d_{xz}–π back-bonding increases, thus stabilizing the Ni–S bond length. This interpretation is consistent with the observation that the C–C and C–S bond lengths decrease as would be expected upon increasing the electron density in the S-π molecular orbital. Although the exact makeup of the C=O region of the ground-state molecular orbital was not given in the original calculations,[6] it is apparent from our experimental results that the electron density must reside in a region that is highly antibonding in nature.

An alternate way of explaining the experimental results involves the use of valence bond structures.[3] By analogy to the well-known oxalate ion resonance structures, we can draw two forms of the dto^{2-}[20] ion. Clearly, bonding of the electropositive Ni^{2+} ion to dto^{2-}

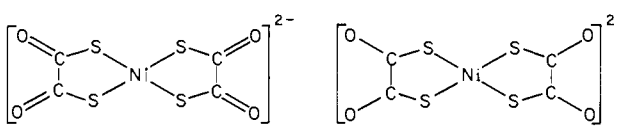

I II

will favor structure I and indeed the C=O stretching frequency of red $K_2[Ni(dto)_2]$ is ca. 20 cm^{-1} higher than the corresponding mode in free dto^{2-}.[18] On the other hand, addition of the electropositive $SnCl_4$ to the oxygen side will favor structure II, causing a decrease in the ν(C=O) frequency while increasing the frequency of the coupled ν(C—C) + ν(C—S) mode.

Visible Spectra and Excitation Profiles. Figures 8 and 9 show the electronic spectra of the red and black forms of $K_2[Ni(dto)_2]$ along with excitation profiles for the coupled C–C + C–S and Ni–S stretching modes. The absorption spectrum of the former is in good agreement with that obtained previously.[6] Molecular

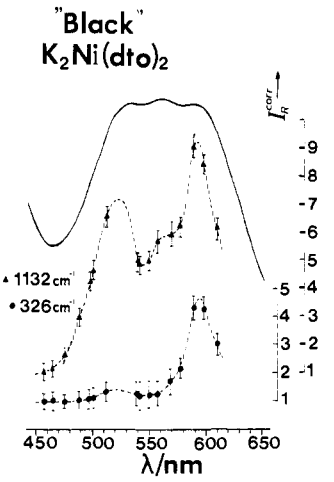

Figure 9. Excitation profiles and electronic spectrum of black $K_2[Ni(dto)_2]$.

orbital calculations by Latham et al. indicated that this low energy envelope was due to a combination of d–d and d–π^* transitions.[6] Although their calculated order of filled metal orbitals terminated in $3b_{3g}(yz) \sim 4a_g(x^2 - y^2) > 3b_{2g}(xz)$, they chose to place the $3b_{3g}$ orbital nearer to the $3b_{2g}$ in order to account for the observed intensities of the lowest energy transitions. Figure 8 is an excellent example of the utility of RR excitation profiles in resolving broad electronic bands into their components, a fact that we have referred to in the past.[19,20] Latham and co-workers[6] claim that three transitions lie underneath the visible absorption envelope of red $K_2[Ni(dto)_2]$. However, only two components are evident in the observed spectrum while the excitation profile of the 1073-cm^{-1} band shows the existence of three distinct peaks. The black form of the complex is interesting in that the three visible transitions are easily discernible in its absorption spectrum (see Figure 9) as well as in the excitation profile of the 1132-cm^{-1} band. The intensities of the totally symmetric ν(C=O) bands near 1600 (red form) and 1500 cm^{-1} (black form) (although not shown in Figures 8 and 9) exhibit enhancement on resonance with all three electronic transitions in the visible region, implying that the molecular orbitals extend well out onto the C=O moieties. Depolarization ratios of all resonance enhanced bands are close to $^1/_3$ when measured at or near the electronic absorption band maxima. This result is indicative of the single state "A"-type enhancement which is typically observed for molecules whose major axes possess less than 3-fold symmetry.[20] Thus we conclude that the three maxima which occur in the excitation profiles arise from three independent charge-transfer transitions.

In their study of the SnX_4 (X = F, Cl, Br, or I) adducts of $Ni(dto)^{2-}$, Coucouvanis et al.[3] reversed the positions of the $4a_g$ and $3b_{3g}$ orbitals in order to explain their results in a manner consistent with the known properties of the planar anionic thiolenes.[21] Although we cannot unequivocally choose between the two proposed orders, we can place some restrictions on the true configuration based upon the results of our excitation profiles. Neglecting the resonance denominators, the RR intensity will be determined by the square of the integral product $\langle g|\sigma|e\rangle\langle e|\rho|g\rangle\cdot\langle i|v\rangle\langle v|j\rangle$ where g and e refer to the ground and excited electronic states, respectively, σ and ρ refer to Cartesian coordinates, and i, v, and j are letters designating vibrational wave functions. The excitation profies in Figures 8 and 9 are unusual in that the greatest enhancement does not occur at or near the maximum of the absorption envelope. (We reiterate at this point that the spectra have been corrected for self-absorption.[22]) This

(17) Shupack, S. I.; Billig, E.; Clark, R. J. H.; Williams, R.; Gray, H. B. *J. Am. Chem. Soc.* **1964**, *86*, 4594.
(18) Stork, W.; Mattes, R. *Angew. Chem.* **1975**, *87*, 452.
(19) Clark, R. J. H.; Turtle, P. C.; Strommen, D. P.; Streusand, B.; Kincaid, J.; Nakamoto, K. *Inorg. Chem.* **1977**, *16*, 84.
(20) Streusand, B.; Kowal, A. T.; Strommen, D. P.; Nakamoto, K. *J. Inorg. Nucl. Chem.* **1977**, *39*, 1767.
(21) McCleverty, J. A. *Prog. Inorg. Chem.* **1968**, *10*, 49.
(22) Inagaki, F.; Tasumi, M.; Miyazawa, T. *J. Mol. Spectrosc.* **1974**, *50*, 286.

can only mean that the Franck–Condon factors for the vibrational wavefunctions, the latter two integrals, in the lowest energy transitions must be significantly larger than those associated with the higher energy transitions. Therefore the true configuration must be consistent with this observation.

Conclusion

We have investigated two polymorphic forms of $K_2[Ni(dto)_2]$ using IR and RR spectroscopy. Through the use of metal-isotope substitution and normal coordinate treatment, definitive assignments of vibrational frequencies have been made for the red form of the complex. These assignments have allowed us to detect small changes in bond lengths within the first coordination sphere of the Ni complexes which were not evident in the X-ray data. Resonance Raman excitation profiles of the red form of the complex clearly defined the three electronic transitions proposed earlier by Latham et al.[6] Furthermore, the unusual nature of the excitation profiles of the red complex places a useful restriction on the order of the highest occupied molecular orbitals. Finally, overtone sequences of the fundamental ν_1 mode and a combination mode involving ν_1 of the red complex have allowed us to calculate the anharmonicity constant for ν_1.

Acknowledgment. This work was partly supported by the National Science Foundation (CHE-7915169). We wish to express our sincere thanks to Professor D. F. Shriver of Northwestern University who kindly measured the far-infrared spectra of the title compounds.

Interactions of $CpM'(CO)_3^-$ (M' = Cr, Mo, W) with Cations: Effects on CO Exchange and RX Addition Reactions

Marcetta Y. Darensbourg,*† Pedro Jimenez,† James R. Sackett,† John M. Hanckel,† and Robin L. Kump‡

Contribution from the Departments of Chemistry, Tulane University, New Orleans, Louisiana 70118, and Indiana University, Bloomington, Indiana 47405. *Received June 11, 1981*

Abstract: Solution structures of Li^+, Na^+, K^+, Me_4N^+, PPN^+, and $M^+(HMPA)_x$ salts of $CpM'(CO)_3^-$ (M' = Cr, Mo, W) in tetrahydrofuran have been defined by analysis of their ν(CO) IR spectra. Interaction of alkali cations with one carbonyl oxygen is apparent. For the large bis(triphenylphosphine)iminium and HMPA solvated cations, which conductivity measurements showed to exist as associated ion pairs in THF, a non-cation-perturbed, C_{3v}, $CpM'(CO)_3^-$ ion structure exists in solution. The Me_4N^+ cation strongly interacts with the carbonylates; however, the symmetry of the perturbed $CpM'(CO)_3^-$ could not be established. Small amounts (ca. 20 equiv) of the good alkali cation complexing agent HMPA were required to solvent-separate ion pairs of $M^+CpM'(CO)_3^-$ in THF, whereas 400 equiv of CH_3CN was required to achieve a similar environment for the $CpM'(CO)_3^-$. Force constant calculations showed that Li^+ caused the greatest reorganization of electron density in the contact ion paired $CpMo^-(CO)_2(CO\cdots Li^+)$ as contrasted to symmetrically solvated $CpMo(CO)_3^-$; however, the lifetime of such ion-pair interactions is short on the NMR time scale as shown by both C-13 and O-17 NMR studies. Carbon-13 labeled CO exchange into $CpMo(CO)_3^-$ was found to be counterion dependent with rates decreasing as $Li^+ > Na^+ > PPN^+$. The presumed intermediate, coordinatively unsaturated $[CpMo(CO)_2^-]$, was readily scavenged by ^{13}CO but not by phosphine ligands. The nonactivated RX molecules *n*-BuI and *n*-BuBr were found to undergo halide displacement by symmetrically solvated $CpMo(CO)_3^-$, in typical S_N2 fashion, more rapidly than with the contact ion pairs $CpMo^-(CO)_2Co\cdots Na^+$. For RX = BzlCl, the opposite counterion effect was observed. Finding no evidence for radical intermediates, a cation-assisted transition-state formation was asserted for the reaction $Na^+CpMo(CO)_3^- + BzlCl \rightarrow CpMo(CO)_3Bzl$.

Introduction

Over the past 10 years a considerable body of knowledge has accrued regarding the solution structures of highly reactive and important transition metal carbonylates. In a classic group of experiments, the use of $Co(CO)_4^-$ as a probe of solution environment about alkali cations evolved into a rigorous study of the sites of carbonylate ion pairing in various solvents.[1,2] Others have been concerned with the redistribution of electronic charge in the carbonylate itself upon changing the electrostatic potential of the countercations,[3-8] or to ion-pair site specificity in nonsymmetric carbonylates.[3,5,6] The ability of ν(CO) infrared spectroscopy to detect very small structural and electronic changes as well as the availability of a substantial arsenal of appropriate solid-state structural studies of metal carbonylates has promoted the development of a new subdiscipline in ion-pairing phenomena.

The reactivity of transition metal carbonylates is of import to both organic[9] and organometallic[10] synthesis and to catalysis. Early studies established a nucleophilicity scale which had its experimental origins in kinetic studies of the reaction of carbonylates with alkyl halides, monitored by electrochemical methods.[11] The rate expression was rate = $k_2[M'CO^-][RX]$, and a relative comparison of second-order rate constants was set forth as the nucleophilicity scale: $CpFe(CO)_2^-$ (7×10^7) > $CpNi(CO)^-$ (5.5×10^6) > $CpW(CO)_3^-$ (550) > $Mn(CO))_5^-$ (77) > $CpMo(CO)_3^-$ (67) > $CpCr(CO)_3^-$ (4) > $Co(CO)_4^-$ (1, reference).[11] The nucleophilicity scale has quite possibly been used to correlate more data than any other physical organometallic study carried out to date.

†Tulane University.
‡Indiana University.

(1) Edgell, W. F. "Ions and Ion Pairs in Organic Reactions"; Szwarc, M., Ed.; Wiley: New York, 1972; Vol. 1, and references therein. Edgell, W. F.; Hegde, S.; Barbetta, A. *J. Am. Chem. Soc.* **1978**, *100*, 1406.
(2) Edgell, W. F.; Chanjamsri, S. *J. Am. Chem. Soc.* **1980**, *102*, 147.
(3) Darensbourg, M. Y.; Darensbourg, D. J.; Burns, D.; Drew, D. A. *J. Am. Chem. Soc.* **1976**, *98*, 3127.
(4) Pribula, C. D.; Brown, T. L. *J. Organomet. Chem.* **1974**, *71*, 415.
(5) Darensbourg, M. Y.; Darensbourg, D. J.; Barros, H. L. C. *Inorg. Chem.* **1978**, *17*, 297.
(6) Darensbourg, M. Y.; Hanckel, J. M. *J. Organomet. Chem.* **1981**, *217*, C9. Darensbourg, M. Y.; Hanckel, J. M. *Organometallics 1982*, 1, 82.
(7) Pannell, K. H.; Jackson, D. *J. Am. Chem. Soc.* **1976**, *98*, 4443.
(8) Nitay, M.; Rosenblum, M. *J. Organomet. Chem.* **1977**, *136*, C23.
(9) Collman, J. P.; Finke, R. G.; Cawse, J. N.; Brauman, J. I. *J. Am. Chem. Soc.* **1978**, *100*, 4766.
(10) King, R. B. *Acc. Chem. Res.* **1970**, *3*, 417.
(11) Dessy, R. E.; Pohl, R. L.; King, R. B. *J. Am. Chem. Soc.* **1966**, *88*, 5121.

0002-7863/82/1504-1521$01.25/0